

Estimation of Absolute Magnitude-dependent Galactic Model Parameters In Intermediate Latitude With SDSS and SCUSS

Yunpeng Jia^{1*}, Cuihua Du¹, * Zhenyu Wu², Xiyan Peng², Jun Ma², Xu Zhou²,
Xiaohui Fan³, Zhou Fan², Yipeng Jing⁴, Zhaoji Jiang², Michael Lesser³, Jundan Nie²,
Edward Olszewski³, Shiyin Shen⁵, Jiali Wang², Hu Zou², Tianmeng Zhang², Zhimin Zhou²

¹*School of physics, University of the Chinese Academy of Sciences, Beijing 100049, P. R. China*

²*Key Laboratory of Optical Astronomy, National Astronomical Observatories, Chinese Academy of Sciences, Beijing, 100012, China*

³*Department of Astronomy and Steward Observatory, University of Arizona, Tucson, Arizona, USA*

⁴*Department of Physics and Astronomy, Shanghai Jiao Tong University, Shanghai 200240*

⁵*Shanghai Astronomical Observatory, Chinese Academy of Sciences, Shanghai 200030*

Received

ABSTRACT

Based on SDSS and South Galactic Cap of u-band Sky Survey (SCUSS) early data, we use star counts method to estimate the Galactic structure parameters in an intermediate latitude with 10,180 main-sequence (MS) stars in absolute magnitude interval of $4 \leq M_r \leq 13$. We divide the absolute magnitude into five intervals: $4 \leq M_r < 5$, $5 \leq M_r < 6$, $6 \leq M_r < 8$, $8 \leq M_r < 10$, $10 \leq M_r \leq 13$, and estimate the Galactic structure parameters in each absolute magnitude interval to explore their possible variation with the absolute magnitude. Our study shows the parameters depend on absolute magnitude. For the thin disk, the intrinsic faint MS stars have large local space density and they tend to stay close to the Galactic plane. A plausible explanation is that faint MS stars with long lifetime experience long gravitational interaction time result in a short scaleheight. However, for the thick disk, the parameters show a complex trend with absolute magnitude, which may imply the complicated original of the thick disk. For the halo, the intrinsic faint MS stars have large local density and small axial ratio, which indicate a flattened inner halo and a more spherical outer halo.

Key words: Galaxy: fundamental parameters - Galaxy: disk - Galaxy: halo - Galaxy: structure.

1 INTRODUCTION

The star counts method has been used to study the structure of our galaxy by generations of astronomers. This useful method can provide a measurement of the density distribution of the stellar component of the Galaxy. Since Bahcall & Soneira (1980) fitted observations with two components Galactic model, namely disk and halo, and then improved by Gilmore & Reid (1983) through introducing a third component, namely the thick disk, the star counts method has provided a picture of the standard Galactic model. As the great improvement on data collection over the years, more and more researchers try to refine both the estimation of standard Galactic model parameters and the standard Galactic model to explain the currently available observations well. The better we know the Galactic structure, the better we understand the formation and evolution of the Galaxy.

A simple way to study Galactic structure is assuming a

global smooth structure model of our Galaxy, which is based on the modern of physics, and also on the pioneering work of Eggen, Lynden-Bell & Sandage (1962), who argued that the galaxy formed from a relatively rapid ($\sim 10^8$ years) radial collapse of the protogalactic cloud through studying the correlation between ultraviolet excess, metal abundance, angular momentum and the eccentricity of the Galactic orbit. The astronomers have done lots of works on the smooth structure parameters. We can find elaborate list of the structural parameters of the Milky Way in Table 1 of Chang et al. (2011). We relist these parameters in Table 1 to conveniently find their improvements. Previous works show the estimation of the parameters suffer from the degeneracy (Robin et al. 2000; Chen et al. 2001; Siegel et al. 2002; Phleps et al. 2005; Jurić et al. 2008; Bilir et al. 2008; Chang et al. 2011), which could influence the confidence of the final results, but it is unconvinced to take it as a main reason to explain the spread of values in Table 1. We should notice the sample stars used in researchers' works are different. These parameters depend on both the properties and locations of the sample stars, such as abso-

* E-mail: jiayunpeng11@mails.ucas.ac.cn(Jia); ducuihua@ucas.ac.cn(Du)

lute magnitude (Bilir et al. 2006a,b; Karaali et al. 2007), Galactic longitude (Du et al. 2006; Cabrera-Lavers et al. 2007; Ak et al. 2007b; Bilir et al. 2008; Yaz & Karaali 2010; Chang et al. 2011) and Galactic latitude (Du et al. 2006; Ak et al. 2007a), thus these parameters that they derived could different from each other. The explanation of these dependence is still a topic of debate. The issue is not to give an explanation that could interpret the observation well, but rather to test whether the theory of the Galaxy is reasonable and therefore to answer a given question related to the Galactic formation and evolution.

Recent researches give us more information about the structure of the Galaxy: the Galactic structure is not as smooth as we thought. Many more substructures have been discovered, such as Sagittarius dwarf tidal stream (e.g. Majewski et al. 2003), Monoceros stream (e.g. Newberg et al. 2002), and Virgo overdensity (Jurić et al. 2008). The researches show the Milky Way is a complex and dynamic structure that is still being shaped by the merging of neighboring smaller galaxies, and the dynamic process may plays a crucial role in establishing the galactic structure. These are reviewed in detail by Ivezić, Beers & Jurić (2012) and references therein. Needless to say, the presence of irregular structure make the research about Galactic structure more complex.

We are interested in the global smooth structure of the Galaxy. It can help us to define the irregular structure, and then allow us to study the formation and evolution of our Galaxy. In this paper, based on SDSS and the South Galactic Cap u-band Sky Survey early data (SCUSS), we attempt to study the structure parameters' possible variations with absolute magnitude. We present density function in Sect. 2. The introduction of SDSS and SCUSS and the reduction of the data would be described in Sect. 3. Sect. 4 provide the method we used to determine the parameters. Finally, our main results are discussed and summarized in Sect. 5.

2 DENSITY LAWS

In this study, we adopt the density laws of disk by two exponentials functions in cylindrical coordinates:

$$D_i(x, z) = n_i \exp(-(x - R_\odot)/l_i) \exp(-(|z| - z_\odot)/h_i) \quad (1)$$

where $z = z_\odot + r \sin b$ is the vertical distance to the Galactic plane, b is Galactic latitude, r is photometric distance, z_\odot is the vertical distance of the Sun to the plane (25 pc, Jurić et al. 2008). x is the distance to Galactic center on the plane. R_\odot is the distance of the Sun to Galactic center (8 kpc, Reid 1993). l_i and h_i are the scale-length and scaleheight, respectively, and n_i is the normalized number density at (R_\odot, z_\odot) , suffix i take the values 1 and 2 for thin disk and thick disk, respectively.

The density law for halo used most is the de Vaucouleurs spheroid (1948) which was used to describe the surface brightness profile of elliptical galaxies, known as $r^{1/4}$ law. According to Young (1976), the projection of this law into three dimensions has no simple analytic form, but it can derive the asymptotic expansion at origin and infinity point. Based on it, Bahcall (1986) gave an analytic approximation:

$$\begin{aligned} D_3(R, b, l) = & n_3 (R/R_\odot)^{-7/8} \{ \exp[-10.093(R/R_\odot)^{1/4} + 10.093] \} \\ & \times [1 - 0.08669/(R/R_\odot)^{1/4}], R \geq 0.03R_\odot \\ & \times 1.25(R/R_\odot)^{-6/8} \{ \exp[-10.093(R/R_\odot)^{1/4} + 10.093] \}, R < 0.03R_\odot \end{aligned} \quad (2)$$

where R is Galactocentric distance:

$$\begin{aligned} R &= (x^2 + (z/\kappa)^2)^{1/2}, \\ x &= [R_\odot^2 + R^2 \cos^2 b - 2R_\odot R \cos b \cos l]^{1/2}, \end{aligned}$$

and κ is the axial ratio, b and l are the Galactic latitude and longitude.

3 DATA REDUCTIONS

3.1 SCUSS and SDSS

The South Galactic Cap u-band Sky Survey (SCUSS) is an international cooperative project between National Astronomical Observatories, Chinese Academy of Sciences and Steward Observatory, University of Arizona, USA. The project plan to perform a sky survey of about 3700 square degree field of the south Galactic cap in u band (3508 Å) with the 90 inch (2.3 meter) Bok telescope. And this project will also provide part of the essential input data to the The Large Sky Area Multi-Object Fiber Spectroscopic Telescope (LAMOST) project. The telescope equipped with four $4K \times 4K$ CCD mosaic (64-megapixel) and the field of view is $1.08 \text{ deg} \times 1.03 \text{ deg}$. The exposure time is 5 minutes and the limiting magnitude will reach about 23 mag (signal-to-noise = 5). The u band filter, which been used in SCUSS project, is almost same as SDSS u band filter but has few blue shift and do not need any color items of magnitude conversion between standard SDSS u band and SCUSS u band photometric system at first. By testing the data obtained from previous camera and new 90 Prime camera of BOK telescope, the limiting magnitude of SCUSS u band may be 1.5 mag deeper than SDSS u band and can be calibrated by SDSS u band in about 2/3 of SCUSS field. The SCUSS can be used to study Star formation rate, Galactic interstellar extinction, Galaxy morphology, the Galaxy structure, Quasi-Stellar Object, Variable star and Cosmology. Here we just use the early data to study the Galactic structure, and the SCUSS data is still updating. The detailed survey overview and data reduction about SCUSS are in preparing (Zhou et al. 2014; Zou et al. 2014).

The Sloan Digital Sky Survey (SDSS) is a large international collaboration project, it has obtained deep, multi-color images covering more than a quarter of the sky. The SDSS used a dedicated 2.5-meter telescope at Apache Point Observatory, New Mexico. equipped with two instruments: a CCD camera with $30 \times 2048 \times 2048$ CCDs in five filters (*ugriz*; Fukugita et al. 1996) and two 320 fiber double spectrographs. The flux densities are measured in five bands (*u, g, r, i, z*) with effective wavelengths of 3551, 4686, 6165, 7481 and 8931 Å, respectively. The 95% completeness limits of the images are *u, g, r, i, z* = 22.0, 22.2, 22.2, 21.3, 20.5, respectively (Abazajian et al. 2004). The imaging data are automatically processed through a series of software pipelines to produce a catalogue. The relative photometric calibration accuracy for *u, g, r, i, z* are 2%, 1%, 1%, 1% and 1%, respectively (Padmanabhan et al. 2008). The detailed information about SDSS can be found on the SDSS web site (<http://www.sdss.org>) or one can see the overview of SDSS in e.g. Stoughton et al. (2002), Abazajian et al. (2009) and Aihara et al. (2011).

In Table 2, we list the parameters of SCUSS and SDSS filters. Column (1) represents the ID of SCUSS and SDSS filters, and columns (2) and (3) represent effective wavelengths and full width at half-maximum (FWHM) of six filters, respectively.

H_{z1} (pc)	H_{r1} (kpc)	f_2	H_{z2} (kpc)	H_{r2} (kpc)	f_h	Re(S) (kpc)	κ	Reference
310-325	-	0.0125-0.025	1.92-2.39	-	-	-	-	Yoshii (1982)
300	-	0.02	1.45	-	-	-	-	Gilmore & Reid (1983)
325	-	0.02	1.3	-	0.002	3	0.85	Gilmore (1984)
280	-	0.0028	1.9	-	0.0012	-	-	Tritton & Morton (1984)
125-475	-	0.016	1.18 - 2.21	-	0.0013	3.1*	0.8	Robin & Creze (1986)
300	-	0.02	1	-	0.001	-	0.85	del Rio & Fenkart (1987)
285	-	0.015	1.3 - 1.5	-	0.002	2.36	Flat	Fenkart & Karaali (1987)
325	-	0.0224	0.95	-	0.001	2.9	0.9	Yoshii et al. (1987)
249	-	0.041	1	-	0.002	3	0.85	Kuijken & Gilmore (1989)
350	3.8	0.019	0.9	3.8	0.0011	2.7	0.84	Yamagata & Yoshii (1992)
290	-	-	0.86	-	-	4	-	von Hippel & Bothun (1993)
325	-	0.020-0.025	1.6-1.4	-	0.0015	2.67	0.8	Reid & Majewski (1993)
325	3.2	0.019	0.98	4.3	0.0024	3.3	0.48	Larsen (1996)
250-270	2.5	0.056	0.76	2.8	0.0015	2.44 - 2.75*	0.60 - 0.85	Robin et al. (1996, 2000)
260	2.3	0.74	0.76	3	-	-	-	Ojha et al. (1996)
290	4	0.059	0.91	3	0.0005	2.69	0.84	Buser et al. (1998, 1999)
240	-	0.061	0.79	-	-	-	-	Ojha et al. (1999)
280/267	-	0.02	1.26/1.29	-	-	2.99*	0.63	Phleps et al. (2000)
330	2.25	0.065 - 0.13	0.58 - 0.75	3.5	0.0013	-	0.55	Chen et al. (2001)
-	2.8	3.5	0.86	3.7	-	-	-	Ojha (2001)
280(350)	2 - 2.5	0.06 - 0.10	0.7 - 1.0 (0.9 - 1.2)	3 - 4	0.0015	-	0.50 - 0.70	Siegel et al. (2002)
285	1.97	-	-	-	-	-	-	Lopez-Corredoira et al. (2002)
-	3.5	0.02-0.03	0.9	4.7	0.002-0.003	4.3	0.5-0.6	Larsen & Humphreys (2003)
320	-	0.07	0.64	-	0.00125	-	0.6	Du et al. (2003)
265-495	-	0.052-0.098	0.805-0.970	-	0.0002-0.0015	-	0.6-0.8	Karaali et al. (2004)
268	2.1	0.11	1.06	3.04	-	-	-	Cabrera-Lavers et al. (2005)
300	-	0.04-0.10	0.9	-	-	3/2.5*	1/0.6	Phleps et al. (2005)
220	1.9	-	-	-	-	-	-	Bilir et al. (2006b)
160-360	-	0.033-0.076	0.84-0.87	-	0.0004-0.0006	-	0.06-0.08	Bilir et al. (2006a)
301/259	-	0.087/0.055	0.58/0.93	-	0.001	-	0.74	Bilir et al. (2006c)
220-320	-	0.01-0.07	0.6-1.1	-	0.00125	-	>0.4	Du et al. (2006)
206/198	-	0.16/0.10	0.49/0.58	-	-	-	0.45	Ak et al. (2007a)
140-269	-	0.062-0.145	0.80-1.16	-	-	-	-	Cabrera-Lavers et al. (2007)
220-360	1.65-2.52	0.027-0.099	0.62-1.03	2.3-4.0	0.0001-0.0022	-	0.25-0.85	Karaali et al. (2007)
167-200	-	0.055-0.151	0.55-0.72	-	0.0007-0.0019	-	0.53-0.76	Bilir et al. (2008)
245(300)	2.15(2.6)	0.13(0.12)	0.743(0.900)	3.261(3.600)	0.0051	2.77*	0.64	Jurić et al. (2008)
325-369	1.00-1.68	0.0640-0.0659	0.860-0.952	2.65-5.49	0.0033-0.0039	-	0.489-0.654	Yaz & Karaali (2010)
360	3.7	0.07	1.02	5	0.002	2.6*	0.55	Chang et al. (2011)
103-350	-	0.083-0.165	0.525-0.675	-	0.0005-0.0065	-	0.20-0.84	this work

Table 1. Galactic model parameters tabulated base on the Table 1 in Chang et al. (2011). H_z and H_r mean scaleheight and scalelength, respectively. And suffix 1 and 2 denote thin disk and thick disk, respectively. f_2 and f_h are the local stellar density ratio of the thick-to-thin disk and halo-to-thin disk, respectively. The parentheses are the corrected values for binarism. The asterisk denotes the power-law index replacing Re, which is commonly known as the de Vaucouleurs radius, and κ is axial ratio.

3.2 Choose sample stars

The data used in this work are taken from SCUSS early data and the eighth data release of SDSS (Aihara et al. 2011). We choose 7.07 deg^2 field locate at $50^\circ \leq l \leq 55^\circ, -46^\circ \leq b \leq -44^\circ$. Considering the SDSS CCDs saturated at about $r \sim 14$ mag (Ivezić et al. 2001) and the robust point source-galaxy separation at $r \sim 21.5$ mag (Lupton et al. 2002), we restrict the apparent magnitudes in the range of $15 \leq r \leq 21.5$. As SCUSS can reach deeper magnitude on u-band than SDSS, we use u band data from SCUSS early observation, including apparent magnitude u and the corresponding errors, instead of those from SDSS. The u band magnitude and error mentioned hereafter will be the ones from SCUSS. The total absorptions for each star, A_u, A_g, A_r, A_i, A_z , are taken from SDSS. The apparent magnitudes u, g, r, i, z are de-reddened:

$$u_0 = u - A_u, g_0 = g - A_g, r_0 = r - A_r, i_0 = i - A_i, z_0 = z - A_z$$

All the magnitudes and colors mentioned hereafter will be de-reddened ones.

Star/Galaxy classification base on the ‘type’ parameter provided by SDSS (the value 3 means Galaxy, and 6 means Star), the technical details can be found on the SDSS web site (<http://www.sdss.org>). In Figure 1, we give the two-color diagram $(r - i)_0$ versus $(g - r)_0$ distribution of all stars and the solid line is stellar locus which is described by Eq. 3 (Jurić et al. 2008), the dashed line and the dotted-dashed line are 0.15 mag and 0.3 mag from stellar locus, respectively. As shown in Fig. 1, there are some non-main sequence (non-MS) stars. We apply the method mentioned in Jurić et al. (2008) to remove hot white dwarfs, low-redshift quasars and white dwarf/red dwarf unresolved binaries from our sample. Their procedure consists of rejecting objects at distances larger than 0.3 mag from the stellar locus. But as pointed by Yaz & Karaali (2010), reject-

Filter	Wavelength (Å)	FWHM (Å)
u (SCUSS)	3508	360
u (SDSS)	3551	570
g	4686	1390
r	6165	1370
i	7481	1530
z	8931	950

Table 2. Parameters of SCUSS and SDSS filters. Column (1) represents the ID of SCUSS and SDSS filters, and columns (2) and (3) represent effective wavelengths and full width at half-maximum (FWHM) of six filters, respectively.

ing objects at distance larger than 0.15 mag is appropriate for Galactic latitude $< b > = 45^\circ$. In this study, we reject those objects at distance larger than 0.15 mag. In addition, we also restrict the objects in interval $(g-r)_0 \leq -0.3$ to remove very early MS stars (see Fig. 2 in Yaz & Karaali 2010) and in interval $(r-i)_0 \geq 1.8$ to ensure the photometric parallax method is good enough (see Figure 2 in Jurić et al. 2008).

$$(g-r)_0 = 1.39\{1 - \exp[-4.9(r-i)_0^3 - 2.45(r-i)_0^2 - 1.68(r-i)_0 - 0.05]\} \quad (3)$$

While the two-color diagram of $(u-g)_0$ versus $(g-r)_0$ in Fig. 2(a), show there still exist non-MS stars. We use Eq. 4 to roughly remove those:

$$(u-g)_0 = \exp[-(g-r)_0^2 + 2.8(g-r)_0 - 1] \quad (4)$$

Any point source lie at the distance in vertical direction to the locus that described by Eq. 4 further than 0.6 mag would be rejected. Simultaneously, we reject the point source whose $(u-g)_0$ is smaller than 0.6 mag to roughly remove quasars (see Fig. 9 in Jurić et al. 2008 and Richards et al. 2002).

The absolute magnitude can be derived by photometric parallax method described by Jurić et al. (2008), i.e. the “bright normalization”:

$$M_r = 3.2 + 13.30(r-i)_0 - 11.50(r-i)_0^2 + 5.4(r-i)_0^3 - 0.70(r-i)_0^4 \quad (5)$$

Note that this relation was even constructed with kinematic consideration to reconcile the differences between some relations proposed by different researchers (see Fig. 2 in this paper). We must point that the effect of the metallicity on this photometric parallax relation is hard to correct satisfactorily (Jurić et al. 2008 have illuminated the reason in detail), especially the gradients of the metallicity distribution are exist in Galactic components (e.g. Ivezić et al. 2006; Bilir et al. 2012; Coşkunoğlu et al. 2012; Peng et al. 2012, 2013). After calculating the absolute magnitude, the photometric distance r is derived from the following equation:

$$r_0 - M_r = 5 \log r - 5 \quad (6)$$

In Figure 3, we show the apparent magnitude (r-band) histogram of sample stars. Two arrows show the limited r-magnitude in our work: 15.0 mag for lower limit and 21.5 mag for upper limit.

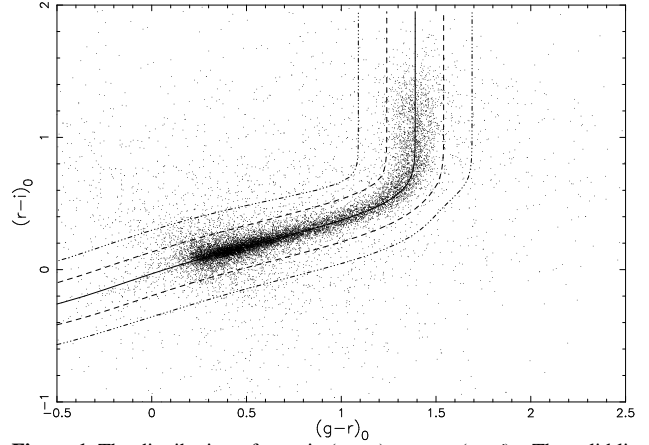


Figure 1. The distribution of stars in $(g-r)_0$ versus $(r-i)_0$. The solid line is stellar locus, the dot-dashed lines means 0.3 mag from stellar locus, and dashed lines means 0.15 mag from stellar locus. In this study, we reject objects further than 0.15 mag from the stellar locus.

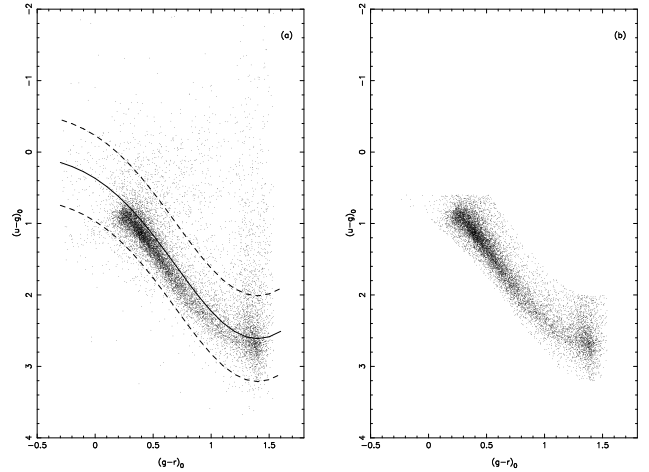


Figure 2. The distribution of stars in $(u-g)_0$ versus $(g-r)_0$ after removing some non-MS stars in $(g-r)_0$ versus $(r-i)_0$. In Figure (a), the solid line described by Eq. 4, and the dashed lines describe the points whose distance in vertical direction to the solid line are 0.6 mag. Figure (b) describe the final distribution of stars in $(u-g)_0$ versus $(g-r)_0$.

The grey area represents the distribution of our final sample stars in absolute magnitude range from 4 mag to 13 mag.

As a summary, the data reduction process should be as precisely as possible to remove non-MS points, but either over reduced or less reduced is exists in practical work. However, as long as the non-MS points are far less than MS stars, we consider the overall distribution of sample stars could smooth the influence caused by non-MS stars, thus it would contribute little to the effect on the determination of parameters.

4 GALACTIC MODEL PARAMETERS

In this study, we choose MS stars in absolute magnitude interval $4 \leq M_r \leq 13$ to estimate the parameters by minimising the reduced χ^2 . All the parameters errors estimations are obtained by increasing χ^2_{min} by 1 (Phleps et al. 2000).

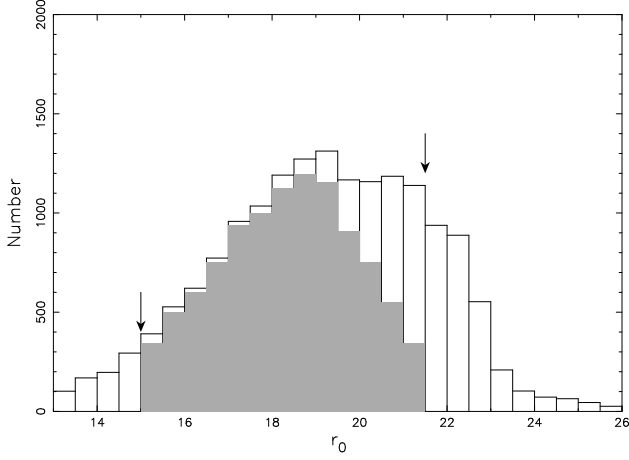


Figure 3. The apparent magnitude histogram of sample stars in r -magnitude. Two arrows show the bright and faint limiting r -magnitudes in our work. The grey area is our final sample stars which distributed in absolute magnitude from 4 mag to 13 mag.

4.1 The procedure used in this work

(i) We divide the absolute magnitude into five intervals: $4 \leq M_r < 5$, $5 \leq M_r < 6$, $6 \leq M_r < 8$, $8 \leq M_r < 10$, $10 \leq M_r \leq 13$, see Table 3. This way of dividing the intervals can ensure enough numbers of sample stars in each interval to explore possible parameters variations with absolute magnitude. (ii) We divide the distance into suitable numbers of logarithmic bins, and then derive the observed number density distribution in each absolute magnitude interval by using the following equations:

$$D(r) = \frac{N(r)}{\Delta V_{12}} \quad (7)$$

$$\Delta V_{12} = \left(\frac{\pi}{180}\right)^2 \frac{\omega}{3} (r_2^3 - r_1^3) \quad (8)$$

$$\sigma_D(r) = \frac{\sqrt{N(r)}}{\Delta V_{12}} \quad (9)$$

where ω denotes the size of the field (unit in deg^2), r_1 and r_2 are lower limit and upper limit of the volume ΔV_{12} , respectively, and N is the number of stars, σ_D is Poisson error of the density due to the shot noise. For every logarithmic distance bin we use the mean height z above the Galactic plane $z_i = \sin b < r_i >$, where $< r_i > = [(r_i^3 + r_{i+1}^3)/2]^{1/3}$. (iii) We obtain the parameters by fitting the model to the observation with χ^2 method. In the last process, we distinguish disk and halo by their spatial distribution if the sample stars in the considered absolute magnitude interval are composed of three components (see Table 3). In this condition, based on the pioneering works (e.g. Reid & Majewski 1993; Bilir et al. 2006a), we take $z = 4$ kpc as the boundary of disk and halo, and simultaneously derive the parameters of thin and thick disk first, then fit thick disk and halo with the overall density distribution using the determined value of thin disk parameters to obtain the parameters of the last two components as final results. Note that the thick disk parameters are derived twice. In order to distinguish between the two ways in obtaining the thick disk parameters, we call the way fitting with thin and thick disks as ‘disk-fitting’, and the way fitting with thick disk and halo as ‘halo-fitting’.

Absolute magnitude	Number	r_{\min}	r_{\max}	component
$4 \leq M_r < 5$	2680	1000 pc	31.6 kpc	thick+halo
$5 \leq M_r < 6$	3213	631 pc	19.9 kpc	thin+thick+halo
$6 \leq M_r < 8$	2568	151 pc	12.6 kpc	thin+thick+halo
$8 \leq M_r < 10$	1258	100 pc	5.0 kpc	thin
$10 \leq M_r \leq 13$	461	25 pc	2.0 kpc	thin

Table 3. Informations about sample stars in each absolute magnitude interval. The second column denotes the number of sample stars. The third and fourth column are the lower and upper limit distance, respectively. The last column means the components we considered in each absolute magnitude interval. Even though the distance can up to 5.0 kpc in interval [8 – 10], the thick disk stars are infrequent, we just consider the thin disk only. The similar condition hold for the thin disk in interval [4 – 5].

4.2 Absolute magnitude-dependent Galactic model parameters

As the scalelength is in magnitude of kiloparsec, compare with scaleheight in parsec (see Table 1), which is so large that contribute little to the change of the density in a small field, as shown in Eq. 1, it has little impact on other parameters, so we roughly evaluate them in absolute magnitude interval $4 \leq M_r \leq 13$ by disk-fitting, and hereafter fix them when obtaining the other parameters in every interval.

Our results shows the values of l_1 and l_2 are in the range of $l_1=2400\text{--}4800$ pc, and $l_2=3600\text{--}6000$ pc, respectively. The poor constraint on scalelength probably due to our sample stars distributed in a narrow radial direction of cylindrical coordinate. As other parameters are insensitive to scalelength for the reason cited above, we take $l_1=3000$ pc and $l_2=5000$ pc in this work, which are roughly equal with the median value of the range they spread.

With the evaluated value of scalelength, we quickly obtain other parameters in each absolute magnitude interval. In order to compare with other researchers’ works, we also obtain the parameters in interval $4 \leq M_r \leq 13$. Our final results of parameters are listed in Table 4.

For the thin disk, with the increase of absolute magnitude, the scaleheight decreases from 350 pc to 103 pc, while the local density increases from $1.25 \times 10^6 \text{ star/kpc}^3$ to $2.32 \times 10^7 \text{ star/kpc}^3$. The above results are consistent with Bilir et al. (2006a) (see Table 6 in that paper). The results reveal a phenomenon for thin disk: the intrinsic faint MS stars tend to stay closer to Galactic plane and have larger local density than that of intrinsic bright MS stars. Consequently, as the contribution of the faint stars in our work, the scaleheight of the thin disk ($h_1=205$ pc) in interval $4 \leq M_r \leq 13$ is smaller than most previous works. As shown in Figure 4, the dependence between the disk parameters is exist in this work. This figure is plotted by disk-fitting in interval $5 \leq M_r < 6$, other intervals also plot similar shape. The cross mark represents the best-fit values of the Galactic model parameters.

However, from Table 4 we notice that the thick disk parameters are non-monotonic change with absolute magnitude. We also notice the dependence between n_2 and h_2 : the larger n_2 , the smaller h_2 . The same dependence also holds between n_1 and h_1 . This is caused by the intrinsic property of Eq. 1: h_2 and n_2 , n_1 and h_1 are anti-correlation. These dependence will emerge when fitting the model to observation, which are also showed in Figure 4. In addition, we can see the dependence between thick disk parameters

M_r (mag)	h_2 (pc)	n_2 (star/kpc ³)	n_2/n_1 (percent)
[5-6]	675 (900)	2.06E(5) (1.44E(5))	16.5 (11.5)
[6-8]	525 (575)	7.17E(5) (6.95E(5))	15.5 (15.0)
[4-13]	595 (697)	1.37E(6) (1.04E(6))	8.25 (6.25)

Table 5. Parameters of thick disk. The values with parenthesis are obtained by disk-fitting, and those without parenthesis are obtained by halo-fitting.

in Figure 5, which is plotted by the halo-fitting. For the disk-fitting, the scaleheight h_2 and local density normalized to thin disk n_2/n_1 is 900 pc and 0.115, respectively, in absolute magnitude interval $5 \leq M_r < 6$. While for the halo-fitting, h_2 and n_2/n_1 is 675 pc and 0.165, respectively. The comparison of the two sets of parameters is listed in Table 5. Notice that the scaleheight of halo-fitting is always smaller than disk-fitting, this is caused by the contribution from the halo stars at large distance in the disk-fitting, which can overestimate the scaleheight. We can also notice that the large discrepancy exists between the two pairs of thick disk parameters in interval $5 \leq M_r < 6$, a possible reason is the degeneracy exists in parameters of halo (see below), which could influence the determination of thick disk parameters (see Figure 5). As the halo-fitting consider the contribution of the halo, thus the parameters obtained in this way are more reliable, so we favor the value of thick disk parameters obtained by halo-fitting than it did by disk-fitting.

For the halo, with the increase of absolute magnitude, the local density n_3 increases from 1.54×10^3 star/kpc³ to 3.01×10^4 star/kpc³, while the axial ratio κ decreases from 0.84 to 0.20 (see Table 4). The large range of κ is also found by Karaali et al. (2007), who gave the range of $0.25 \leq \kappa \leq 0.85$, which is consistent with this work. The results show intrinsic fainter MS stars in halo have larger local density and their distributions are more non-spherical. As large distance can be reached in bright interval, so the values of κ shows the halo is more spherical at large distance, indicates a flattened inner halo and a spherical outer halo. The value of κ in interval $4 \leq M_r \leq 13$ is 0.55, which is closed to the recent results (Du et al. 2006; Bilir et al. 2006a; Jurić et al. 2008; Chang et al. 2011). The contour plot of halo-fitting is shown in Figure 5. In the bottom right of this Figure, κ versus n_3/n_1 shows the degeneracy exist between this two parameters. The similar degeneracy between this two parameters is also found in interval $6 \leq M_r < 8$ and $4 \leq M_r \leq 13$, but not found in interval $4 \leq M_r < 5$. Needless to say, the degeneracy could influence the parameters of the thick disk and halo in this work.

Figure 6 shows the observed and evaluated space density functions combined for the considered components which corresponding to these listed in Table 3. In this figure, the corresponding absolute magnitude intervals are $4 \leq M_r < 5$, $5 \leq M_r < 6$, $6 \leq M_r < 8$, $8 \leq M_r < 10$, $10 \leq M_r \leq 13$, $4 \leq M_r \leq 13$.

5 SUMMARY AND DISCUSSION

We estimate the Galactic model parameters using χ^2 method in absolute magnitude intervals: $4 \leq M_r < 5$, $5 \leq M_r < 6$, $6 \leq M_r < 8$, $8 \leq M_r < 10$, $10 \leq M_r \leq 13$, with a unique density law for each population individually of 7.07 deg^2 field locate at $50^\circ \leq l \leq 55^\circ$, $-46^\circ \leq b \leq -44^\circ$, to explore their possible variation with absolute magnitude from SDSS and SCUSS photometry. We also estimate

the parameters in absolute magnitude interval $4 \leq M_r \leq 13$ in order to compare with other researchers' works. Our results show the parameters are absolute magnitude dependent (see Table 4). This is a possible reason to explain why different researchers obtained different parameters.

5.1 Thin disk

The local density of the thin disk increases and the scaleheight decreases, with the sample stars get fainter. The local density $n_1(R_\odot, z_\odot)$ varies from 1.25×10^6 star/kpc³ in absolute magnitude interval $5 \leq M_r < 6$ to 2.32×10^7 star/kpc³ in absolute magnitude interval $10 \leq M_r \leq 13$, and the scaleheight changes from 350 pc to 103 pc in the corresponding absolute magnitude interval. The results reveal a phenomenon for thin disk: the intrinsic faint MS stars tend to stay closer to the Galactic plane, and have larger local density. In order to compare with other researchers' results, we derive the scaleheight of the thin disk in absolute magnitude interval $4 \leq M_r \leq 13$, that is 205 pc, which is a little smaller than most previous work (see Table 1). As these parameters depend on absolute magnitude, we can conclude that the small scaleheight of thin disk in absolute magnitude interval $4 \leq M_r \leq 13$ is caused by the contribution of the faint MS stars in our sample.

It is obvious that different types of MS stars could have experienced different dynamic process, thus could have different specific distributions. In other words, the specific distribution of MS stars could dependent on absolute magnitude. The quantitative calculation to explain this phenomenon may need the chemical, kinematic and dynamic information, the star formation history and star formation rate may also be included. Here we just give a possible qualitative explanation: bright MS stars have large mass and short lifetime which lead the local density to be relatively smaller than that of the faint one, thus the gravitational interaction time they experienced are short, this may make the bright MS stars stay a little further in mean than the fainter one, so the scaleheight h_1 of the bright MS stars would be larger.

5.2 Thick disk

The final results of the thick disk suffer from the degeneracy between the two halo parameters: κ and n_3 , see Figure 5. It raise the uncertainty of the relationship between thick disk parameters and absolute magnitude. **As our local density of thin disk n_1 changes with absolute magnitude, it is significative to compare the value of n_2 with other works rather than n_2/n_1 . The values of h_2 we obtained are a little smaller than previous works, thus the value of n_2 (normalized at (R_\odot, z_\odot)) should be a little larger. As shown in Table 4, h_2 roughly fall into the range of $520 < h_2(\text{pc}) < 680$, simultaneously, n_2 roughly fall into the range of $2.0 \times 10^5 < n_2(\text{star/kpc}^3) < 1.4 \times 10^6$. The results show the parameters of thick disk are non-monotonic change with absolute magnitude, which may imply the origin of the thick disk is complicated.**

5.3 Halo

As shown in Table 4, the halo parameters κ and n_3 are monotonic change with absolute magnitude. The axial ratio κ varies from 0.84 in bright interval to 0.20 in faint interval which indicates a flattened inner halo and a more spherical halo. The trend of n_3 shows intrinsic faint MS stars have large local density.

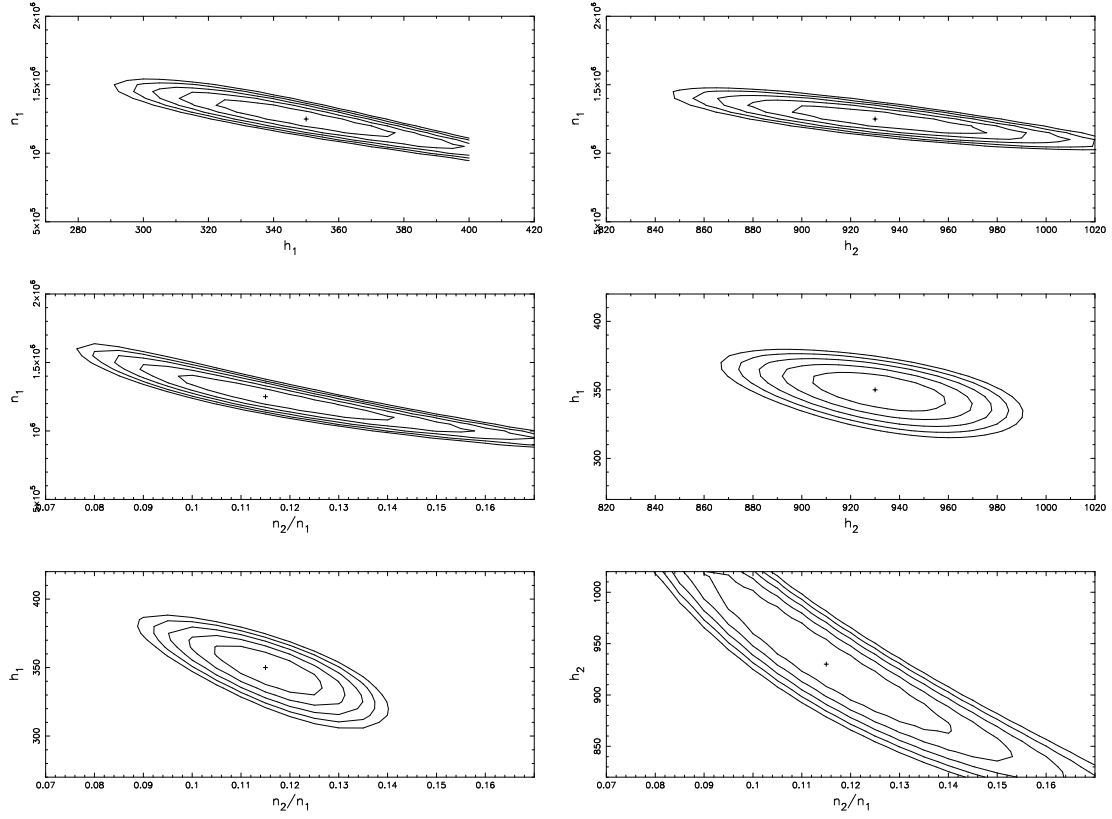


Figure 4. Contour plotted of the χ^2 value of pairs of disk (thin and thick disk) parameters in absolute magnitude interval $5 \leq M_r < 6$. The cross mark represents the best-fit values of the Galactic model parameters.

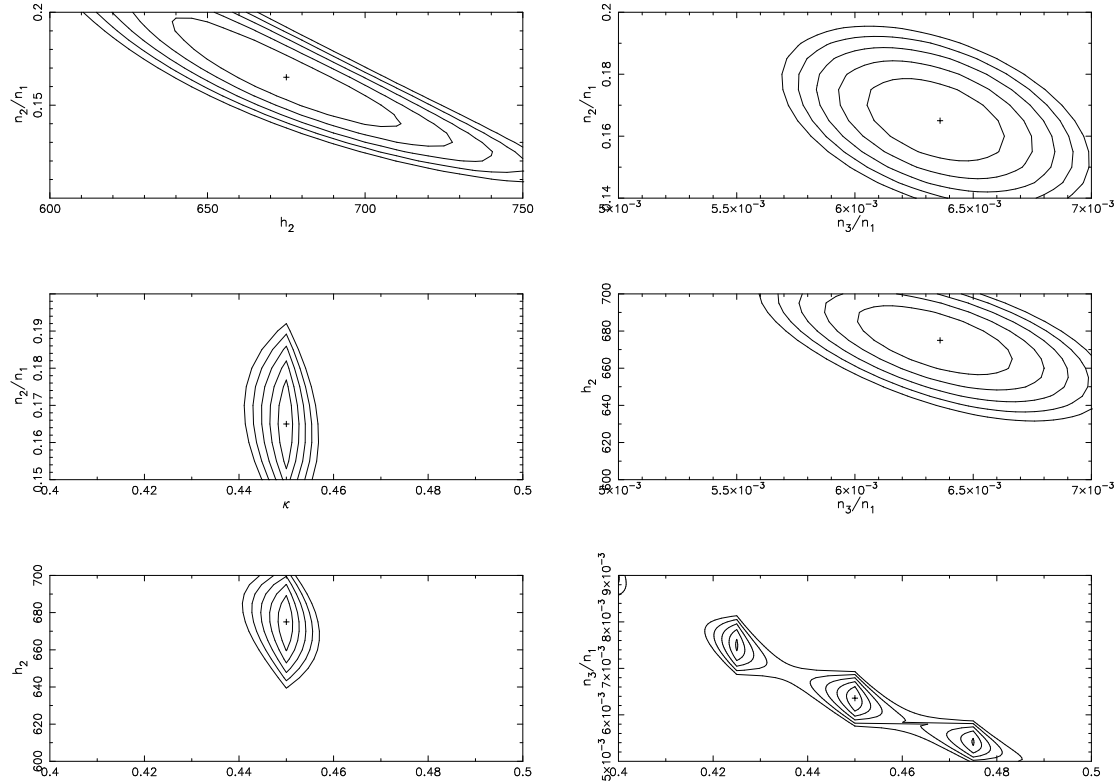


Figure 5. Contour plotted of the χ^2 value of pairs of thick disk and halo parameters in absolute magnitude interval $5 \leq M_r < 6$. The cross mark represents the best-fit values of the Galactic model parameters.

M_r (mag)	$n_1(R_\odot, Z_\odot)$ (star/kpc ³)	h_1 (pc)	$n_2(R_\odot, Z_\odot)$ (star/kpc ³)	h_2 (pc)	n_2/n_1 (percent)	$n_3(R_\odot, Z_\odot)$ (star/kpc ³)	κ	n_3/n_1 (percent)
[4 – 5]			$(4.35^{+0.48}_{-0.47})E(5)$	575^{+20}_{-20}		$(1.54^{+0.14}_{-0.15})E(3)$	$0.84^{+0.020}_{-0.040}$	
[5 – 6]	$(1.25^{+0.05}_{-0.05})E(6)$	350^{+10}_{-10}	$(2.06^{+0.32}_{-0.31})E(5)$	675^{+30}_{-35}	$16.5^{+2.50}_{-2.50}$	$(7.95^{+0.70}_{-0.75})E(3)$	$0.45^{+0.025}_{-0.025}$	$0.64^{+0.06}_{-0.06}$
[6 – 8]	$(4.63^{+0.25}_{-0.28})E(6)$	194^{+12}_{-12}	$(7.17^{+0.70}_{-0.69})E(5)$	525^{+15}_{-15}	$15.5^{+1.50}_{-1.50}$	$(3.01^{+0.65}_{-0.60})E(4)$	$0.20^{+0.025}_{-0.025}$	$0.65^{+0.14}_{-0.13}$
[8 – 10]	$(1.31^{+0.10}_{-0.09})E(7)$	180^{+5}_{-4}						
[10 – 13]	$(2.32^{+0.27}_{-0.27})E(7)$	103^{+5}_{-5}						
[4 – 13]	$(1.66^{+0.08}_{-0.07})E(7)$	205^{+7}_{-7}	$(1.37^{+0.13}_{-0.12})E(6)$	595^{+15}_{-15}	$8.25^{+0.75}_{-0.75}$	$(8.23^{+1.65}_{-1.64})E(3)$	$0.575^{+0.025}_{-0.025}$	$0.05^{+0.01}_{-0.01}$

Table 4. The Galactic model parameters obtained in this study. n_i and h_i are local density and scaleheight for the thin and thick disks, respectively. κ is axial ratio of the halo. Suffix 1,2,3, denote thin disk, thick disk, halo, respectively. n_2/n_1 and n_3/n_1 are the normalization density for thick disk and halo, respectively.

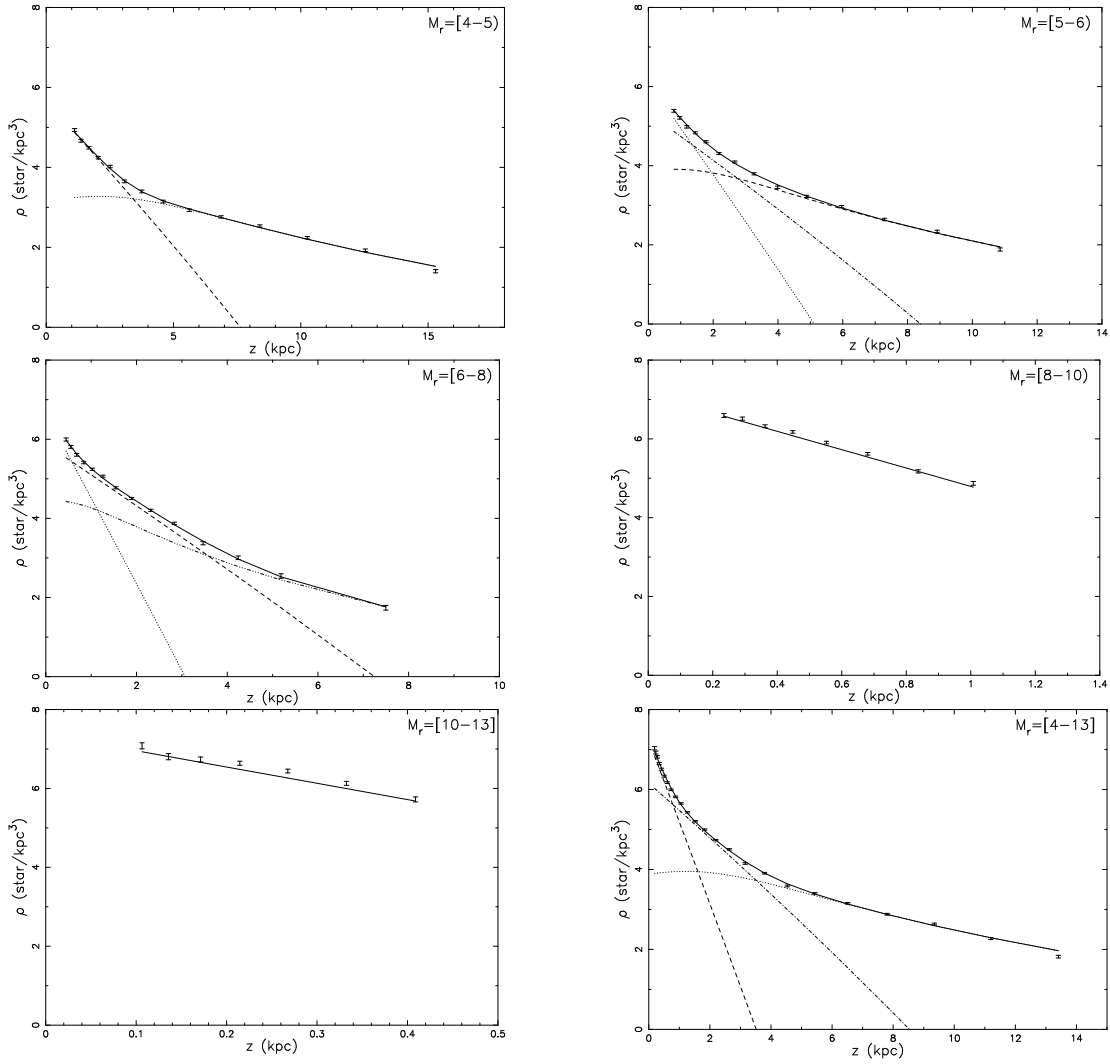


Figure 6. Observed (dots with error bars) and evaluated (solid line) space density functions combined for the considered population components which corresponding to these listed in Table 4.

In general, the values of χ^2 for halo-fitting are larger than disk-fitting in all intervals. Figure 6 can reflect the large deviation of halo-fitting. The deviation may come from the influence of the uncompleted data, especially at large distance.

As seen in Figure 5, the degeneracy exists between the halo

parameters n_3 and κ . So the confidence of the halo parameters monotonic change with absolute magnitude will be influenced. We do not know what cause the halo parameters degenerate, but the most likely reason is the unsatisfactory of the halo component fitting: whether the observation is not good enough (e.g. the incom-

plete data in halo component) or the halo model is not precisely describe the Galaxy.

In summary, we fit the observations with three components Galactic model to estimate the Galactic structure parameters to explore their possible variations with absolute magnitude. Our results show the parameters of the thin disk and halo are monotonic change with absolute magnitude, but the thick disk is non-monotonic. The explanation of this phenomenon need more work. Also, we still need a new method to estimate the Galactic structure parameters in order to break the degeneracy. As greatly improve on data collection and more and more researchers work on these field in recent years, we believe these questions can be solved in the near future. We still have a long way to know our galaxy well.

ACKNOWLEDGMENTS

We especially thank the referee, S. Bilir, for his insightful comments and suggestions which have improved the paper significantly. This work was supported by joint fund of Astronomy of the the National Nature Science Foundation of China and the Chinese Academy of Science, under Grants U1231113. This work was also supported by the GUCAS president fund and the Chinese National Natural Science Foundation grant No. 11373033. This work has been supported by the Chinese National Natural Science Foundation through grants 11373035, and by the National Basic Research Program of China (973 Program), No. 2014CB845702.

We would like to thank all those who participated in observations and data reduction of SCUSS for their hard work and kind cooperation. The SCUSS is funded by the Main Direction Program of Knowledge Innovation of Chinese Academy of Sciences (No. KJCX2-EW-T06). It is also an international cooperative project between National Astronomical Observatories, Chinese Academy of Sciences and Steward Observatory, University of Arizona, USA. Technical supports and observational assistances of the Bok telescope are provided by Steward Observatory. The project is managed by the National Astronomical Observatory of China and Shanghai Astronomical Observatory.

Funding for SDSS-III has been provided by the Alfred P. Sloan Foundation, the Participating Institutions, the National Science Foundation, and the U.S. Department of Energy Office of Science. The SDSS-III web site is <http://www.sdss3.org/>.

SDSS-III is managed by the Astrophysical Research Consortium for the Participating Institutions of the SDSS-III Collaboration including the University of Arizona, the Brazilian Participation Group, Brookhaven National Laboratory, Carnegie Mellon University, University of Florida, the French Participation Group, the German Participation Group, Harvard University, the Instituto de Astrofísica de Canarias, the Michigan State/Notre Dame/JINA Participation Group, Johns Hopkins University, Lawrence Berkeley National Laboratory, Max Planck Institute for Astrophysics, Max Planck Institute for Extraterrestrial Physics, New Mexico State University, New York University, Ohio State University, Pennsylvania State University, University of Portsmouth, Princeton University, the Spanish Participation Group, University of Tokyo, University of Utah, Vanderbilt University, University of Virginia, University of Washington, and Yale University.

REFERENCES

- Abazajian K. et al., 2009, *ApJS*, 182, 543
 Aihara H. et al., 2011, *ApJS*, 193, 29
 Ak S., Bilir S., Karaali S., Buser R., 2007a, *AN*, 328, 169
 Ak S., Bilir S., Karaali S., Buser R., Cabrera-Lavers A., 2007b, *NewA*, 12, 605
 Bahcall J. N., 1986, *ARA&A*, 24, 577
 Bahcall J. N., Soneira R. M., 1980, *ApJS*, 44, 73
 Bilir S., Karaali S., Gilmore G., 2006a, *MNRAS*, 366, 1295
 Bilir S., Karaali S., Ak S., Yaz E., Hamzaoglu E., 2006b, *NewA*, 12, 234
 Bilir S., Karaali S., Güver T., Karataş Y., Ak S. G., 2006c, *Astron. Nachr.* 327, 72
 Bilir S., Cabrera-Lavers A., Karaali S., Ak S., Yaz E., López-Corredoira M., 2008, *PASA*, 25, 69
 Bilir S., Karaali S., Ak S., Önal Ö., Dağtekin N. D., Yontan T., Gilmore G., Seabroke G. M., 2012, *MNRAS*, 421, 3362
 Buser R., Rong J., Karaali S., 1998, *A&A*, 331, 934
 Buser R., Rong J., Karaali S., 1999, *A&A*, 348, 98
 Cabrera-Lavers A., Garzón F., Hammersley P. L., 2005, *A&A*, 433, 173
 Cabrera-Lavers A., Bilir S., Ak S., Yaz E., López-Corredoira M., 2007, *A&A*, 464, 565
 Chang C. K., Ko C. M., Peng T. H., 2011, *ApJ*, 740, 34
 Chen B. et al. 2001, *ApJ*, 553, 184
 Coşkunoğlu B., Ak S., Bilir S., Karaali S., Önal Ö., Yaz E., Gilmore G., Seabroke G. M., 2012, *MNRAS*, 419, 2844
 de Vaucouleurs G., 1948, *AnAp*, 11, 247
 del Rio G., Fenkart R., 1987, *A&AS*, 68, 397
 Du C. H., Zhou X., Ma J., 2003, *A&A*, 407, 541
 Du C. H., Ma J., Wu Z. Y., Zhou X., 2006, *MNRAS*, 372, 1304
 Eggen O. J., Lynden-Bell D., Sandage A. R., 1962, *ApJ*, 136, 748
 Fenkart R., Karaali S., 1987, *A&AS*, 69, 33
 Fukugita M., Ichikawa T., Gunn J. E., Doi M., Shimasaku K., Schneider D. P., 1996, *AJ*, 111, 1748
 Gilmore G., 1984, *MNRAS*, 207, 223
 Gilmore G., Reid N., 1983, *MNRAS*, 202, 1025
 Ivezić Ž., Beers T. C., Jurić M., 2012, *ARA&A*, 50, 251
 Ivezić Ž. et al. 2001, *AJ*, 122, 2749
 Ivezić Ž. et al., 2006, *Mem. Soc. Astron. Italiana*, 77, 1057
 Jurić M. et al., 2008, *ApJ*, 673, 864
 Karaali S., Bilir S., Hamzaoglu E., 2004, *MNRAS*, 355, 307
 Karaali S., Bilir S., Yaz E., Hamzaoglu E., Buser R., 2007, *PASA*, 24, 208
 Kuijken K., Gilmore G., 1989, *MNRAS*, 239, 605
 Larsen J. A., 1996, PhD thesis, Univ. Minnesota
 Larsen J. A., Humphreys R. M., 2003, *AJ*, 125, 1958
 Lopez-Corredoira M., Cabrera-Lavers A., Garzon F., Hammersley P. L. 2002, *A&A*, 394, 883
 Lupton R. H. et al. 2002, *Proc. SPIE*, 4836, 350
 Majewski S. R., Skrutskie M. F., Weinberg M. D., Ostheimer J. C., 2003, *ApJ*, 599, 1082
 Newberg H. J., et al., 2002, *ApJ*, 569, 245
 Ojha D. K., 2001, *MNRAS*, 332, 426
 Ojha D. K., Bienaymé O., Mohan V., Robin A. C., 1999, *A&A*, 351, 945
 Ojha D. K., Bienaymé O., Robin A. C., Creze M., Mohan V., 1996, *A&A*, 311, 456
 Padmanabhan N. et al. 2008, *ApJ*, 674, 1217
 Peng X. Y., Du C. H., Wu Z. Y., 2012, *MNRAS*, 422, 2756
 Peng X. Y., Du C. H., Wu Z. Y., Ma J., Zhou X., 2013, *MNRAS*, 434, 3165

- Phleps S., Drepper S., Meisenheimer K., Fuchs B., 2005, *A&A*, 443, 929
- Phleps S., Meisenheimer K., Fuchs B., Wolf C., 2000, *A&A*, 356, 108
- Reid M. J., 1993, *ARA&A*, 31, 345
- Reid N., Majewski S. R., 1993, *ApJ*, 409, 635
- Richards G. T., 2002, *AJ*, 123, 2945
- Robin A. C., Creze M., 1986, *A&A*, 157, 71
- Robin A. C., Reyl  C. Cr    M., 2000, *A&A*, 359, 103
- Robin A. C., Haywood M., Creze M., Ojha D. K., Bienayme O., 1996, *A&A*, 305, 125
- Siegel M. H., Majewski S. R., Reid I. N., Thompson I. B., 2002, *ApJ*, 578, 151
- Stoughton C. et al., 2002, *AJ*, 123, 485
- Tritton K. P., Morton D. C., 1984, *MNRAS*, 209, 429
- von Hippel T., Bothun G. D., 1993, *ApJ*, 407, 115
- Yamagata T., Yoshii Y., 1992, *AJ*, 103, 117
- Yaz E., Karaali S., 2010, *NewA*, 15, 234
- Yoshii Y., 1982, *PASJ*, 34, 365
- Yoshii Y., Ishida K., Stobie R. S., 1987, *AJ*, 93, 323
- Young P. J., 1976, *AJ*, 81, 807